ELSEVIER

Journal of Alloys and Compounds 436 (2007) 131–141

Journal of ALLOYS AND COMPOUNDS

www.elsevier.com/locate/jallcom

Experimental investigation of the Mg–Al–Ca system

M. Aljarrah [a], M. Medraj [a,*], X. Wang [a], E. Essadiqi [b], A. Muntasar [c], G. Dénès [c]

[a] *Mechanical Engineering Department, Concordia University, Montreal, Canada*
[b] *CANMET-MTL, Ottawa, Canada*
[c] *Chemistry Department, Concordia University, Montreal, Canada*

Received 25 May 2006; received in revised form 7 July 2006; accepted 7 July 2006
Available online 22 August 2006

Abstract

This work focuses on the experimental investigation of the ternary Mg–Al–Ca system using differential scanning calorimetry (DSC), X-ray diffraction (XRD) and metallographic techniques. DSC has permitted real time measurement of the temperature and enthalpy of the phase transformations. One of the invariant transformations predicted by thermodynamic modeling was verified experimentally and found to occur at 513 °C with composition close to 10.8 at.% Ca, 79.5 at.% Mg and 9.7 at.% Al. Three binary compounds are found to have an extended solid solubility into the ternary system: (Mg_2Ca) where Al substitute Mg in the binary compound Mg_2Ca, (Al_2Ca) and (Al_3Ca_8) where Mg substitute Al in the binary compounds Al_2Ca and Al_3Ca_8, respectively. Two morphologies of eutectic structure were observed in the micrographs and supported by solidification curves; a coarse and fine eutectic microstructures due to the existence of Al_2Ca and Mg_2Ca, respectively.

Keywords: Mg–Al–Ca ternary system; Phase diagram; Thermal analysis; X-ray diffraction; Microstructure; Thermodynamics

1. Introduction

Magnesium has the best strength to weight ratio of common structural metals, and it has exceptional die-casting characteristics. This makes magnesium alloys particularly attractive for transportation applications such as in the automotive and aircraft industries for weight reduction and higher fuel efficiency. The rapid growth in the magnesium consumption [1–4] has highlighted the need for a greater understanding of factors that influence the properties of magnesium alloys and industry's increasing demands for a wider range of magnesium alloys with lower thermal expansion, higher fatigue strength, higher creep strength, and better corrosion resistance [3,4]. The current use of magnesium in automotive applications is limited to non-critical parts because of its restricted creep properties. Rare earths additions improve creep resistance of Mg alloys by forming precipitates, but the main drawback of using these elements is their high cost [5].

A large amount of effort has been made to increase the service temperature of the Mg alloys [6–8]. The addition of Ca element has been reported in recent years to replace the cost intensive rare earth metals. It is well known that the addition of Ca up to 0.3% increases ductility through grain size refinement [9]. The improvement of creep resistance is attributed to the thermal stability and the interface coherency of the Mg_2Ca and Al_2Ca precipitates with the Mg matrix. Calcium additions also protect the melt surface combined with less slag formation and additive loss. And the resulting alloys show lower secondary creep rates and higher tensile strength than AZ91 combined with comparable castability and good melt handling [5,7,10–13].

However, to date little effort has been made to construct the phase relationships of the Mg–Al–Ca system. The limited number of publications on this system mainly focuses on the thermodynamic calculation and/or experimental investigation of the Mg-rich region. These calculations exhibited a considerable discrepancy among the published results and substantial disagreement with experimental data. These discrepancies are because the thermodynamic modeling of the Mg–Al–Ca ternary system did not take into account the ternary phases [14]. Moreover, the accuracy of the thermodynamic model depends on the reliability of the experimental data. Therefore, parallel to the thermodynamic calculation work, there is a great need for sufficient and reliable experimental data for the reoptimization of this system.

* Corresponding author. Tel.: +1 514 848 2424x3146; fax: +1 514 848 3175.
E-mail address: mmedraj@encs.concordia.ca (M. Medraj).

0925-8388/$ – see front matter © 2006 Elsevier B.V. All rights reserved.
doi:10.1016/j.jallcom.2006.07.034

Table 1
The studied samples with the corresponding phase fields

Group	Samples	Phase field [15]
#1	1–5	(Mg) + Al_2Ca + γ
#2	6–13	(Mg) + Al_2Ca + Mg_2Ca
#3	14–17	Al_2Ca + γ+Al
#4	18–20	Mg_2Ca + Al_2Ca + $Al_{14}Ca_{13}$
#5	21	Mg_2Ca + Al_2Ca + Al_3Ca_8

2. Experimental

Twenty-one samples were chosen by critical assessment of the experimental and thermodynamic datasets that are available in the literature. Table 1 and Fig. 1 show the different investigated samples and their phase fields that were predicted by thermodynamic calculations based on the model of Islam and Medraj [15]. Special attention was focused on the Mg-rich corner because of the interest in the Mg alloys. Since, Mg_2Ca and Al_2Ca give the thermodynamic stability to the Mg—Al—Ca system, samples containing these phases were chosen. In addition, three samples in Mg-rich region were chosen to verify the eutectic point reported in Refs. [15–17]. All the thermodynamic calculations were performed using FactSage 5.3 [18].

Mg—Al—Ca alloys were prepared by melting stoichiometric amounts of the constituent elements in an induction-melting furnace under argon with 1%SF_6 (sulfur hexafluoride) to protect the melt from oxidation. In preparing the alloys, magnesium of 99.8 wt.%, aluminum of 99.9 wt.% and calcium of 99 wt.% purities were used. The isothermal section of the Mg—Al—Ca system at room temperature with the investigated compositions in weight percentage is given in Fig. 1. The actual chemical composition was measured quantitatively by ICP atomic emission spectrometry. It was noticed that there is a difference between the nominal and actual compositions, which is due to the low recovery of Ca during melting. Nevertheless, the actual composition was used in the analysis during this work.

Thermal investigation of the Mg—Al—Ca system was performed using a Setaram Setsys DSC-1200 instrument. Temperature calibration of the DSC equipment was done using pure Mg and Al. The samples were cut and mechanically polished to remove any possible contaminated surface layers. Afterwards, they were cleaned with acetone and placed in a graphite crucible with a lid cover to contain Mg vapours and protect the apparatus. To avoid oxidation, multiple evacuations followed by rinses with pure argon, were done. The DSC measurements were carried with heating and cooling rates of 5 °C/min. Slower heating rates were tried and were not found to reveal additional thermal arrests. The weight of the sample was 40–50 mg. During the calibration, it was made certain that the geometrical dimensions, the mass (40–80 mg) and the surface quality did not show any visible effects on DSC spectra. The reproducibility of every measurement was confirmed by collecting the data during three heating and cooling cycles. The estimated error between the repetitive heating and cooling is ±1 °C or less. However, the solidification behavior can be revealed much better with the cooling scans.

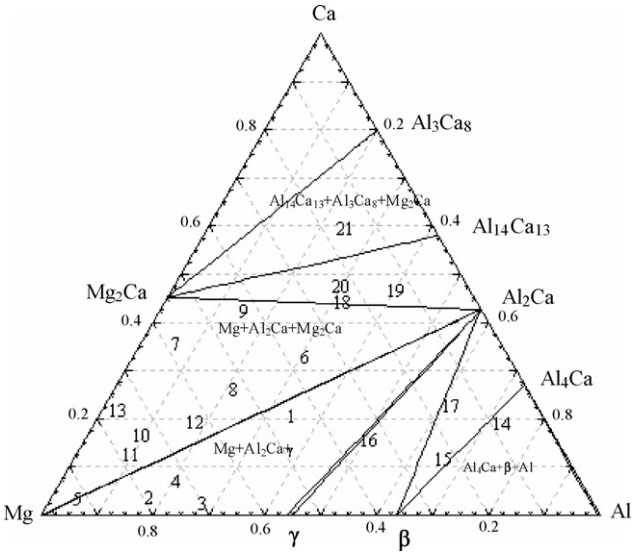

Fig. 1. Mg—Al—Ca ternary isothermal section at 25 °C, based on the thermodynamic modeling of [15], showing the investigated compositions in wt.%.

Phase identification was carried out by X-ray diffraction (XRD) with a Philips diffractometer (Cu Kα radiation) equipped with a PW 1050/25 focusing goniometer with steps 0.02° of 2θ diffraction angle and 1 s exposure time. All the 21 samples were investigated in the powder form in the as-cast condition at room temperature. For the calibration of the X-ray diffractometer, powder was made from pure Mg supplied by Noranda and diffraction patterns were obtained and compared with the literature. The relative peak intensity and the position matched completely. The obtained diffraction patterns were refined and analyzed using Rietveld method in comparison with simulated X-ray spectra using PowderCell 2.3 [19]. The patterns were examined for known oxide phases such as MgO, Al_2O_3 and $MgAl_2O_4$ for any possible oxide formation. Microstructural observations were made using optical microscope (Olympus BX60M). The samples were etched using 1 vol.% nital solution (HNO_3 in ethanol) for a short period of time (~5 s).

Phase assemblage diagrams and vertical sections have been drawn from the database provided in Ref. [15]. The phase assemblage diagram shows the phase transformation temperature during thermal session as well as the relative amount of each phase at any temperature which in turn serves as a guidance to understand the DSC patterns. The vertical section shows the sequence of the thermal events during heating or cooling, whereas the isothermal section presents the phases in equilibrium at room temperature.

3. Results and discussion

3.1. Samples in the (Mg) + Al_2Ca + γ phase field

Five samples have been studied in the (Mg) + Al_2Ca + γ region as shown in Fig. 1. The DSC heating and cooling curves of sample 1 (20.43/44.79/34.78 wt.%Ca/Mg/Al) are shown in Fig. 2(a). Two exotherms appear in the cooling curve at 442 and 523 °C, which correspond to the two endotherms that appear in the heating spectrum at 472 and 540 °C. Another exothermic signal was revealed on the cooling curve at 750 °C, but did not appear in the heating spectrum. It can be seen from this figure that the peaks appear to be more distinct in the cooling than in the heating curve. This is due to the supercooling effect that causes more grain nucleation and more energy accumulation.

Fig. 2(b) shows the calculated vertical section of sample 1 with DSC signals from the cooling curve. The measured transformation temperatures correspond to the three phase boundaries in the vertical section: L/L + Al_2Ca/L + Al_2Ca + (Mg)/Al_2Ca + (Mg) + γ. Moreover, the formation of (Mg) during solidification process takes place within a temperature range of around 50 °C whereas it is more than 300 °C for Al_2Ca as shown in Fig. 2(c). This leads to greater amount of nucleation for (Mg) than for Al_2Ca during cooling, which causes higher system enthalpy change. This results in a stronger and broader second peak in the cooling curve at 523 °C as shown in Fig. 2(a). The DSC and XRD measurements along with the thermodynamic calculations of sample 1 are summarized in Table 2.

While analyzing X-ray diffraction for most of the investigated samples, shifting of Mg, Al_2Ca, Mg_2Ca and Al_3Ca_8 peaks suggest the existence of solid solutions which will be denoted

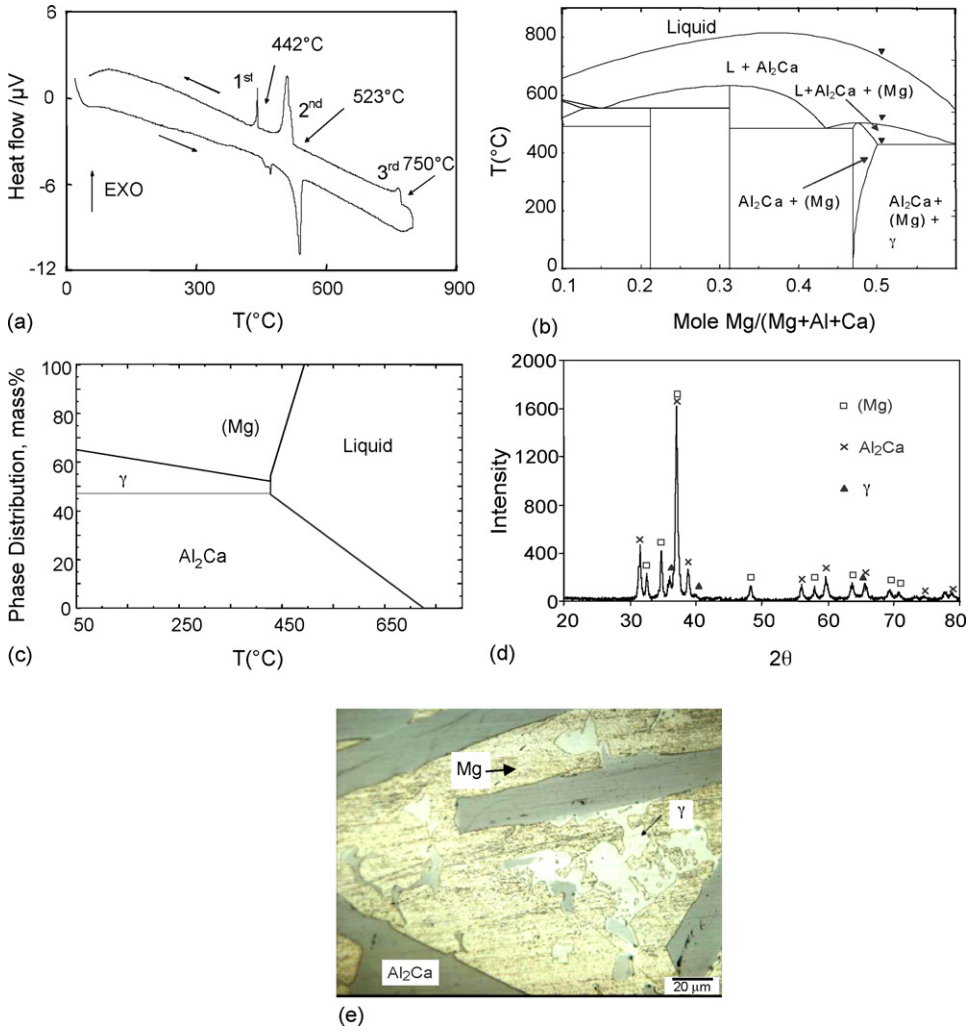

Fig. 2. (a) DSC spectra; (b) the calculated vertical section at constant 35.4 at.% Al with DSC signals from cooling curve; (c) phase assemblage diagram; (d) XRD pattern and (e) optical micrograph of sample 1 (20.43/44.79/34.78 wt.% Ca/Mg/Al).

Table 2
Phase contents identified by XRD at 25 °C and DSC measurements with thermodynamic calculation of the investigated samples in the (Mg) + Al_2Ca + γ phase field (c denotes cooling and h denotes heating)

Sample	Identified phases using XRD	DSC thermal signals (°C)	Thermodynamic calculation based on the database reported in Ref. [15]	
			T (°C)	Reactions or phase boundary
1	(Mg), (Al_2Ca) and γ	472h/442c	430	(Mg) + Al_2Ca + γ/(Mg) + Al_2Ca + L
		540h/523c	496	(Mg) + Al_2Ca + L/Al_2Ca + L
		750c	728	Al_2Ca + L/L
2	(Mg), (Al_2Ca) and γ	442h/431c	427	(Mg) + Al_2Ca + γ/Al_2Ca + (Mg) + L
		–	485	Al_2Ca + (Mg)/(Mg) + L
		556h/542c	539	(Mg) + L/L
3	(Mg), (Al_2Ca) and γ	441h/431c	428	(Mg) + Al_2Ca + γ/Al_2Ca + (Mg) + L
		–	450	Al_2Ca + (Mg)/(Mg) + L
		488h/460c	476	(Mg) + L/L
4	(Mg), (Al_2Ca) and γ	445c	428	(Mg) + Al_2Ca + γ/Al_2Ca + (Mg) + L
		524c	494	Al_2Ca + (Mg)/(Mg) + L
		584c	502	(Mg) + L/L
5	(Mg) and (Al_2Ca)	–	195	(Mg) + Al_2Ca + γ/Al_2Ca + (Mg)
		534h/524c	501	Al_2Ca + (Mg)/(Mg) + L
		585h/605c	616	(Mg) + L/L

through out the text as: (Mg), (Al_2Ca), (Mg_2Ca) and (Al_3Ca_8). The refinement and phase identification of the obtained X-ray patterns were performed using Rietveld method and PowderCell 2.3 program [19]. Fig. 2(d) indicates that sample 1 is composed of (Al_2Ca), (Mg) and traces of γ at room temperature. The plate-like phase shown in Fig. 2(e) is identified as (Al_2Ca) surrounded by (Mg) and small amount of γ. DSC spectra, XRD pattern and optical image are in agreement with the thermodynamic modeling.

The DSC results of samples 2–4 have concurrently verified the invariant phase transformation temperature. The DSC spectra of sample 2 are illustrated in Fig. 3(a). Two peaks appear in the DSC pattern; the first peak featuring a narrow and sharp peak at 431 °C in the cooling session indicating a eutectic transformation. The tail peak at 542 °C represents a univariant reaction and its onset point corresponds to the liquidus. This finding can be correlated with the vertical section in Fig. 2(b). XRD pattern of samples 2–4 identified positively (Mg), (Al_2Ca) and γ as shown in Fig. 2(c) and Table 2. (Al_2Ca) and γ are located at the grain boundaries of the Mg-matrix as shown in Fig. 3(d).

Sample 5 is located in the Mg-rich corner as can be seen in Fig. 1. Two transformations were detected by DSC spectra as shown in Fig. 4(a). The sharp and narrow peak corresponds to the reaction L = (Mg) + Al_2Ca as can be seen from Fig. 4(d). The other peak is broader and tailing back to the baseline that occurs due to solidifying (Mg) from the liquid which is in accordance with Fig. 4(b). The XRD pattern of sample 5 in Fig. 4(c) shows stronger peaks for (Mg) than (Al_2Ca) suggesting that (Mg) has greater relative amount than (Al_2Ca) in this sample. This is in agreement with the phase assemblage diagram and the micrograph of this sample. Also, it can be seen that Mg_2Ca was not detected in the XRD pattern due to its small relative amount. It is worth noting, as can be seen from Fig. 4(f), that the solidification curve deduced from the DSC measurement shows that (Mg) starts to solidify at 605 °C down to 522 °C consuming 75 wt.% of the liquid, then (Al_2Ca) starts solidifying from the remaining liquid forming coarse lamellar structure at the grain boundary of Mg-matrix as can be seen in Fig. 4(e).

3.2. Samples in the (Mg) + Al_2Ca + Mg_2Ca phase field

The microstructure of sample 6 in Fig. 5(a) displays a large amount of plate-like Al_2Ca. There is no distinct shape for Mg_2Ca, and it is probably embedded in the lamellar structure during the invariant transformation that occurs according to L = (Mg) + Mg_2Ca + Al_2Ca at 480 °C as can be seen in Fig. 5(b). XRD pattern identified (Mg), (Mg_2Ca) and (Al_2Ca) positively as shown in Fig. 5(d). Good agreement between XRD and thermodynamic calculations was observed. The DSC spectra of sample 6 are shown in Fig. 5(c), similar spectra were observed for samples 7 and 8 and their results are summarized in Table 3. The sharp and strong peaks occurring at 512, 514 and 519 °C in these three samples, respectively, correspond to the eutectic transformation. (Mg), (Al_2Ca) and (Mg_2Ca) were identified in the XRD patterns of samples 6–8 as can be seen in Fig. 5(d) and Table 3.

A eutectic point in the (Mg) + Mg_2Ca + Al_2Ca field has been investigated through examining samples 10–13. Sample 10 was prepared with the composition of the eutectic point predicted by the thermodynamic modeling of [15–17]. Fig. 6(a and b) show the eutectic transformation that occurs according to L = (Mg) + Al_2Ca + Mg_2Ca.

The DSC spectra of sample 10 in Fig. 6(c) show a sharp, narrow and unique peak which indicates an invariant transformation. The optical micrograph of sample 10 in Fig. 6(d) shows dominated typical lamellar eutectic feature and some plate-like

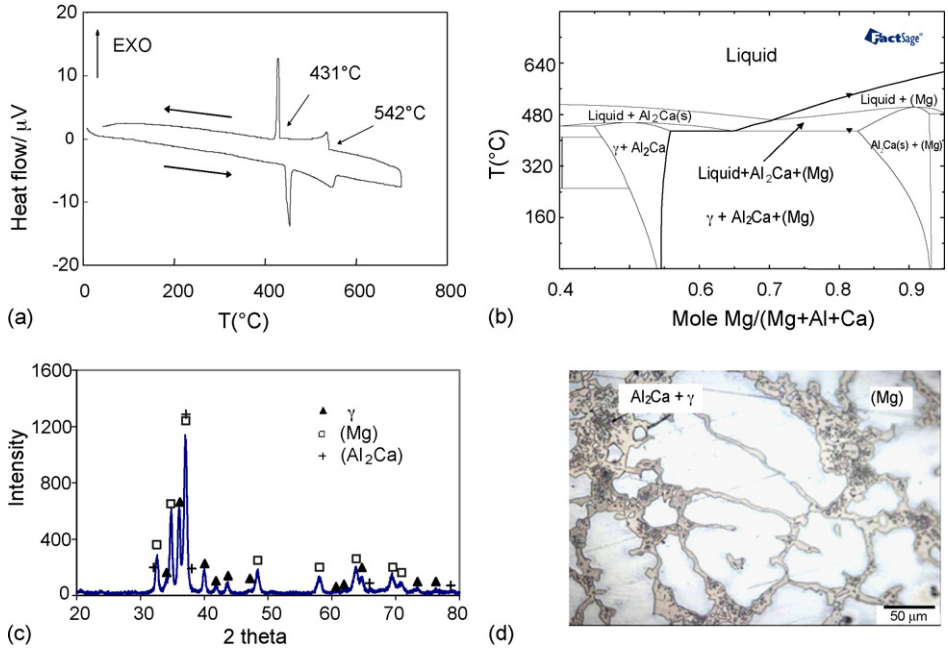

Fig. 3. (a) DSC spectra; (b) the calculated vertical section at 2.3 at.% Ca with DSC signals from cooling curve; (c) XRD pattern and (d) optical micrograph of sample 2 (3.59/78.84/17.57 wt.% Ca/Mg/Al).

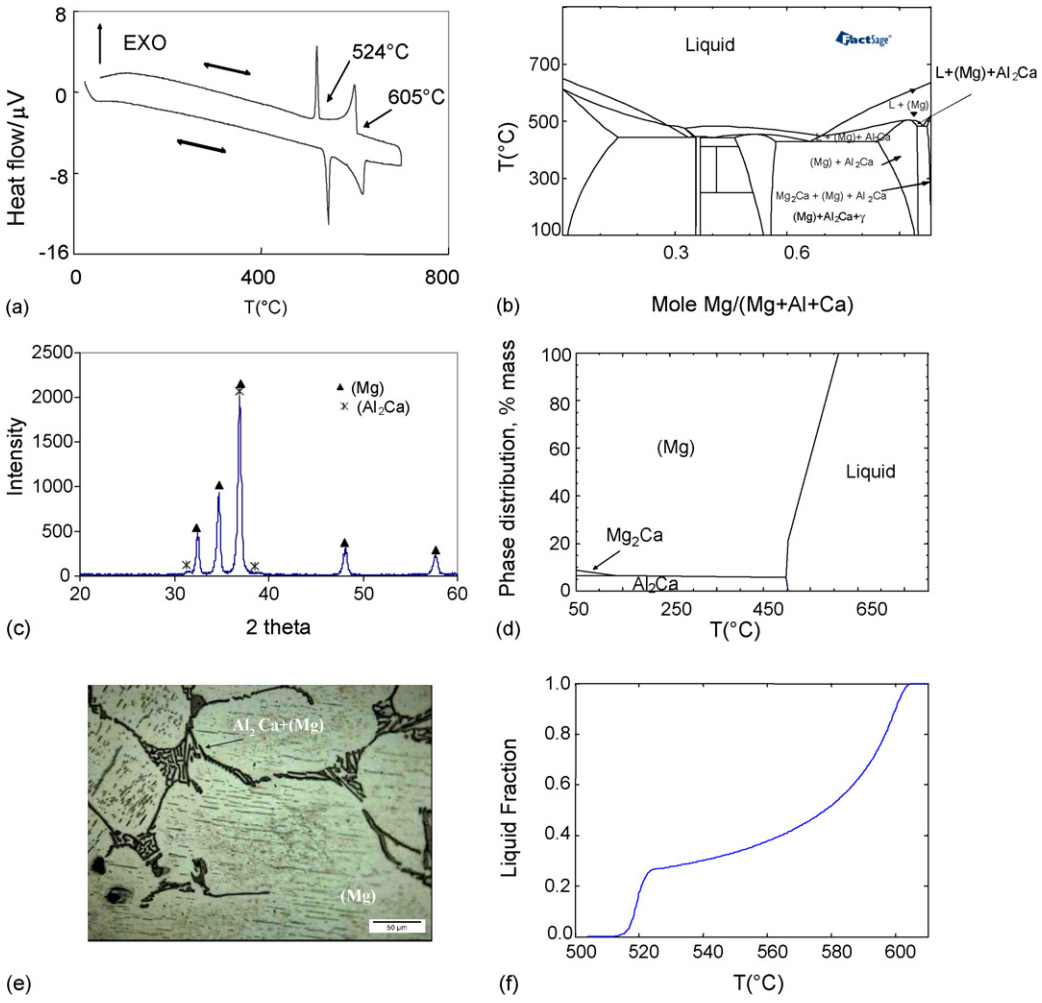

Fig. 4. (a) DSC spectra; (b) the calculated vertical section at 1.7 at.% Ca with DSC signals from cooling curve; (c) XRD pattern; (d) phase assemblage diagram and (e) optical micrograph of sample 5 (2.66/92.17/5.17 wt.% Ca/Mg/Al).

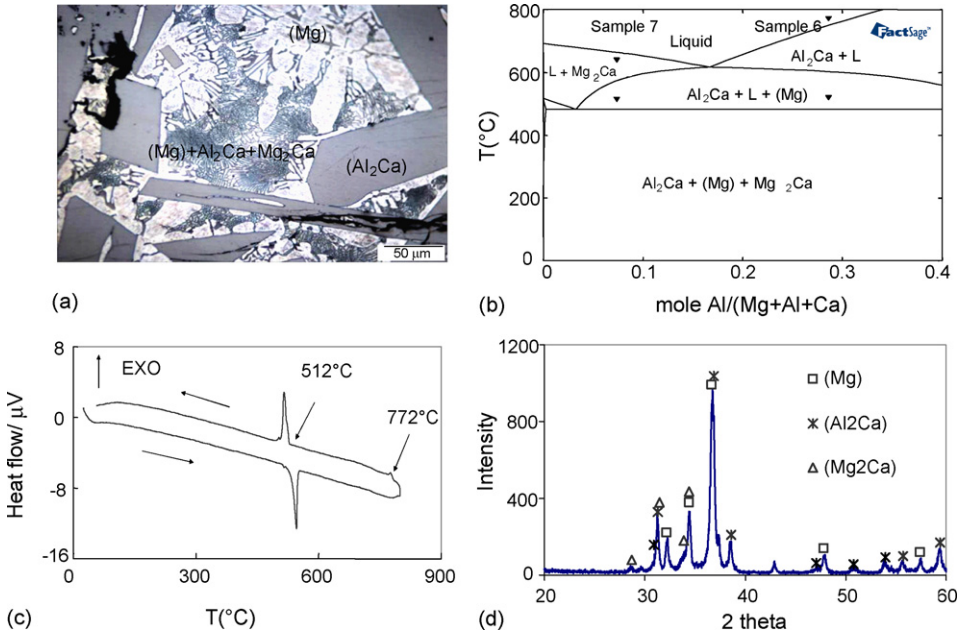

Fig. 5. (a) Optical micrograph; (b) the calculated vertical section at 25.3 at.% Ca with DSC signals from cooling curve; (c) DSC pattern and (d) XRD pattern of sample 6 (32.68/36.30/31.02 wt.% Ca/Mg/Al).

Table 3
Phase contents identified by XRD at 25 °C and DSC measurements with thermodynamic calculation for samples 6–8 (c denotes cooling and h denotes heating)

Sample	Identified phases using XRD	DSC thermal signals (°C)	Thermodynamic calculation based on the database reported in Ref. [15]	
			T (°C)	Reactions or phase boundary
6	(Mg), (Al_2Ca) and (Mg_2Ca)	516h/512c	481	(Mg) + Al_2Ca + Mg_2Ca/Al_2Ca + Mg_2Ca + L
		–	600	Al_2Ca + Mg_2Ca + L/Al_2Ca + L
		772c	748	Al_2Ca/L
7	(Mg), (Al_2Ca) and (Mg_2Ca)	512h/506c	480	(Mg) + Al_2Ca + Mg_2Ca/Al_2Ca + Mg_2Ca + L
		–	569	Al_2Ca + Mg_2Ca + L/Al_2Ca + L
		640h/621c	650	Al_2Ca/L
8	(Mg), (Al_2Ca) and (Mg_2Ca)	514h/519c	482	Al_2Ca + (Mg) + Mg_2Ca/L + Al_2Ca + Mg_2Ca
		–	631	L + Al_2Ca + Mg_2Ca/L + Al_2Ca
		–	666	L + Al_2Ca/L

precipitates. This indicates that the sample is quite close to the eutectic composition.

The XRD pattern in Fig. 6(e) shows the coexistence of the (Mg), (Al_2Ca) and (Mg_2Ca) phases. This is in agreement with the phase assemblage diagram shown in Fig. 6(a). Also, the DSC spectra of sample 13 which is close to samples 11 and 12 detected a transformation temperature at 513 °C which is the eutectic temperature observed in samples 11 and 12. Therefore, it is concluded that the eutectic temperature in this phase field is 513 °C. The DSC and XRD measurements along with the thermodynamic calculations of samples 10–13 are summarized in Table 4. Good agreement can be seen between these results.

The microstructural features of sample 12 show plate-like structure identified as (Al_2Ca), brick-work and lamellar struc-

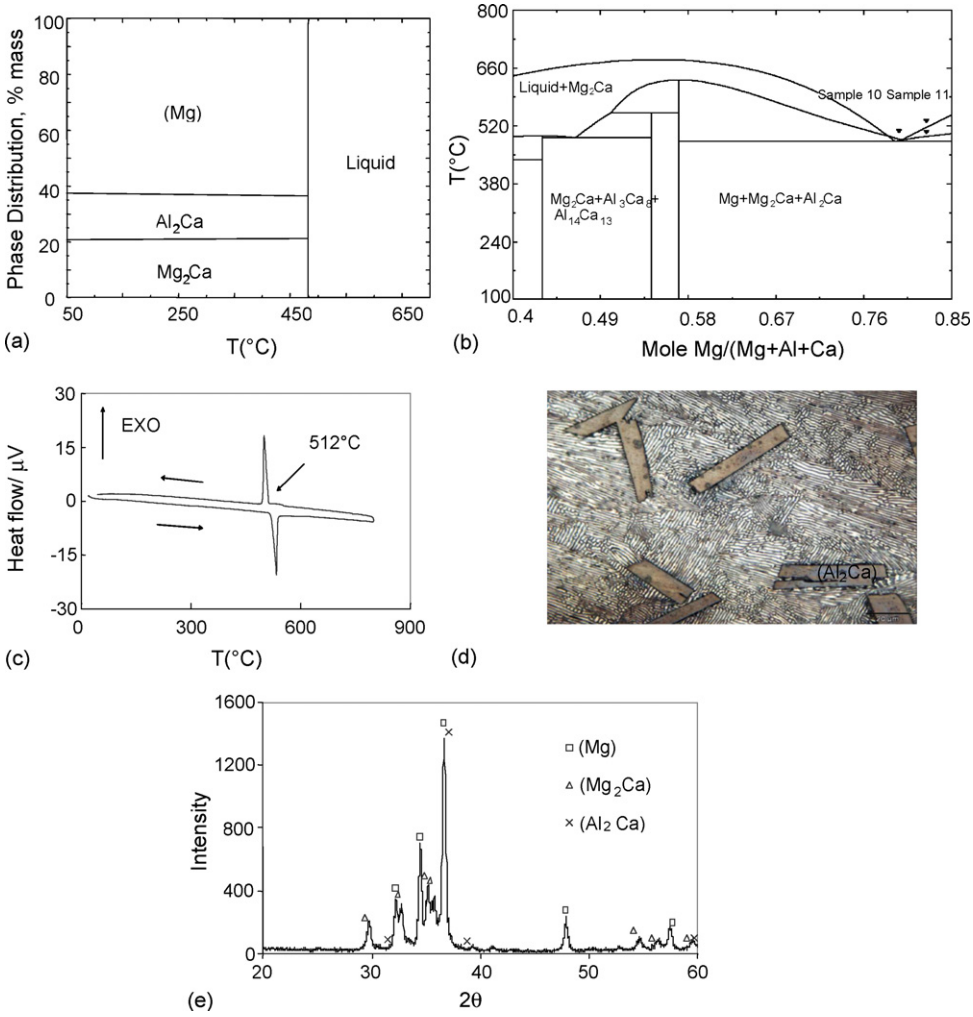

Fig. 6. (a) Phase assemblage diagram; (b) the calculated vertical section at 9.68 at.% Al with DSC signals from cooling curve; (c) DSC pattern; (d) optical micrograph and (e) XRD pattern of sample 10 (16.44/73.61/9.95 wt.% Ca/Mg/Al).

Table 4
Phase contents identified by XRD at 25 °C and DSC measurements with thermodynamic calculation for samples 10–13 (c denotes cooling and h denotes heating)

Sample	Identified phases using XRD	DSC Thermal Signals (°C)	Thermodynamic calculation based on the database reported in Ref. [15]	
			T (°C)	Reactions or phase boundary
10	(Mg), (Al_2Ca) and (Mg_2Ca)	516h/512c	480	L = (Mg) + Al_2Ca + Mg_2Ca
11	(Mg), (Al_2Ca) and (Mg_2Ca)	515h/506c	482	L + (Mg) + Al_2Ca/(Mg) + Al_2Ca + Mg_2Ca
		–	493	L + (Mg)/L + (Mg) + Al_2Ca
		545h/532c	512	L/L + (Mg)
12	(Mg), (Al_2Ca) and (Mg_2Ca)	516h/513c	481	(Mg) + Al_2Ca + Mg_2Ca/Al_2Ca + Mg_2Ca + L
		–	491	Al_2Ca + Mg_2Ca + L/Al_2Ca + L
		678h/626c	587	Al_2Ca/L
13	(Mg), (Al_2Ca) and (Mg_2Ca)	520h/513c	480	(Mg) + Al_2Ca + Mg_2Ca/Mg_2Ca + (Mg) + L
		–	502	Mg_2Ca + (Mg) + L/Mg_2Ca + L
		580h/548c	572	Mg_2Ca + L/L

tures as can be seen in Fig. 7(b). The microstructural features of sample 10 changed to dendrites lamellae in sample 11 as shown in Fig. 7(a) due to the decrease in Ca amount from 16.44 to 12.65 wt.% which resulted in the formation of smaller amounts of (Al_2Ca) and (Mg_2Ca). On the other hand, increasing the amount of Ca from 16.44 to 19.32 wt.%, as in sample 12, enhanced the formation of (Al_2Ca) and (Mg_2Ca) which is clear from the microstructure shown in Fig. 7(b) where the coarse microstructure formed as a result of the transformation at 626 °C due to the precipitation of (Al_2Ca) whereas the fine microstructure occurred as a result of the phase transformation at 513 °C due to the precipitation of (Mg_2Ca) as can be seen from Fig. 7(d).

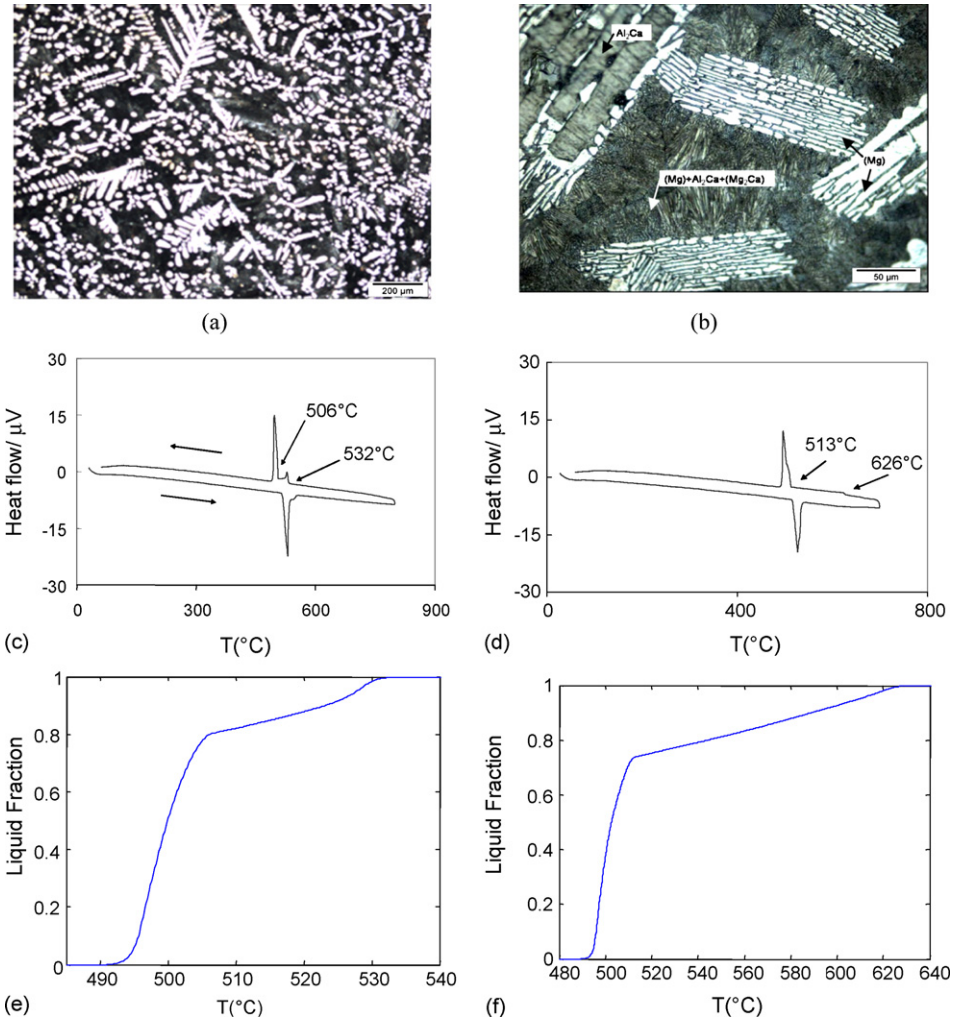

Fig. 7. (a) Optical micrograph of sample 11 (12.65/77.46/9.89 wt.% Ca/Mg/Al); (b) optical micrograph of sample 12 (19.32/62.65/18.04 wt.% Ca/Mg/Al); (c) DSC pattern of sample 11; (d) DSC pattern of sample 12; (e) solidification curve of sample 11 and (f) solidification curve of sample 12.

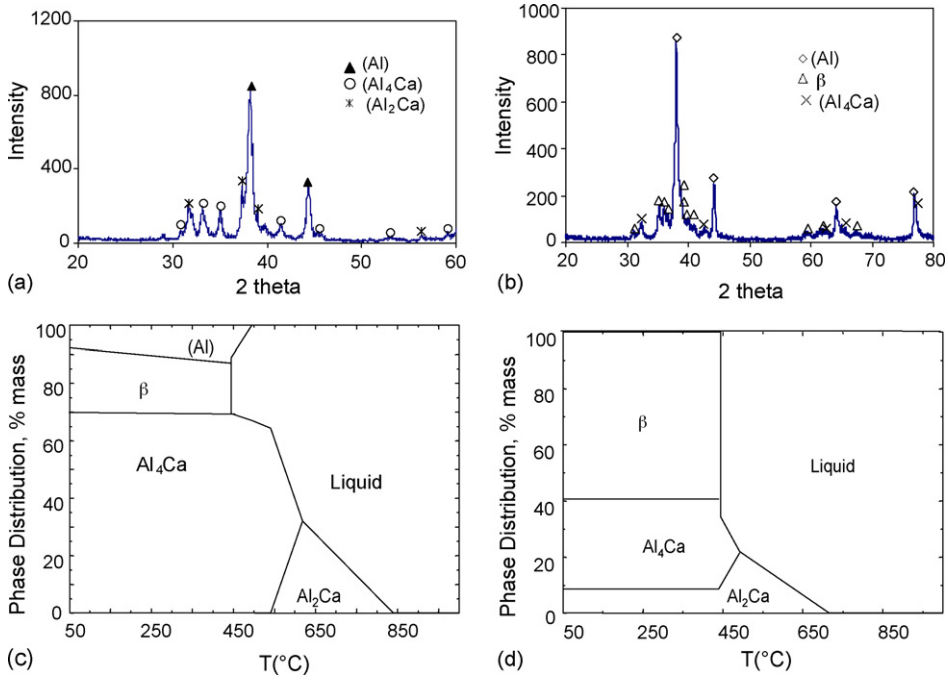

Fig. 8. (a) XRD pattern of sample 14 (19.12/7.91/72.97 wt.% Ca/Mg/Al); (b) XRD pattern of sample 15 (11.67/22.04/66.29 wt.% Ca/Mg/Al); (c) phase assemblage diagram of sample 14 and (d) phase assemblage diagram of sample 15.

Moreover, the solidification curve of sample 12 in Fig. 7(f) shows two phase transformations; one of them occurs at higher temperature forming (Al_2Ca) and the other one forms (Mg_2Ca) in the brick-work and lamellar structures as shown in Fig. 7(b). The slope of the second part of the solidification curve of sample 11 is higher than that of sample 12, which resulted in dendritic structure instead of fine lamellar structures as shown in Fig. 7(e and f).

3.3. Samples in the Al-rich region

Samples 14 and 15 are close to β-Al_4Ca borderline as can be seen in Fig. 1. The XRD patterns of both samples in Fig. 8(a and b) show clearly peaks for (Al) and (Al_4Ca). Sample 14 also contains weak peaks for (Al_2Ca) but there are no peaks for β, whereas sample 15 contains weak peaks for β. This is not consistent with the thermodynamic modeling. The phase assemblage diagram of sample 14 in Fig. 8(c) shows that this sample contains 70 wt.% Al_4Ca at room temperature and Fig. 8(d) shows that sample 15 contains 60 wt.% β at room temperature which does not correspond with the XRD results where Al_4Ca and β did not display strong peaks. This could be due to their low thermal stability. The DSC and XRD measurements along with the thermodynamic calculations for samples 14–17 are summarized in Table 5. It can be seen in this table

Table 5
Phase contents identified by XRD at 25 °C and DSC measurements and calculated transformation temperature of the investigated samples in the Al-rich region (h denotes heating and c denotes cooling)

Sample	Identified phases using XRD	DSC thermal signals (°C)	Thermodynamic calculation based on the database reported in Ref. [15]	
			T (°C)	Reactions or phase boundary
14	(Al), (Al_2Ca) and (Al_4Ca)	–	444	$L + Al_4Ca + (Al)/Al_4Ca + (Al) + \beta$
		–	492	$Al_4Ca + L/L + Al_4Ca + (Al)$
		542c/548h	540	$Al_4Ca + Al_2Ca + L/Al_4Ca + L$
		620c/628h	618	$Al_2Ca + L/Al_4Ca + Al_2Ca + L$
		–	838	$L/Al_2Ca + L$
15	(Al), (Al_4Ca) and β	450c/456h	445	$L + Al_2Ca + A_4Ca/Al_2Ca + Al_4Ca + \beta$
		505c/496h	491	$L + Al_2Ca/L + Al_2Ca + Al_4Ca$
		633c/640h	714	$L/L + Al_2Ca$
16	(Al_2Ca) and β	454c/464h	454	$L + Al_2Ca/Al_2Ca + \gamma$
		774c/783h	752	$L/L + Al_2Ca$
17	(Al_2Ca), γ and β	446c/452h	446	$Al_4Ca + Al_2Ca + L/Al_4Ca + Al_2Ca + \beta$
		488c/482h	469	$Al_2Ca + L/Al_4Ca + Al_2Ca + L$
		–	884	$L/Al_2Ca + L$

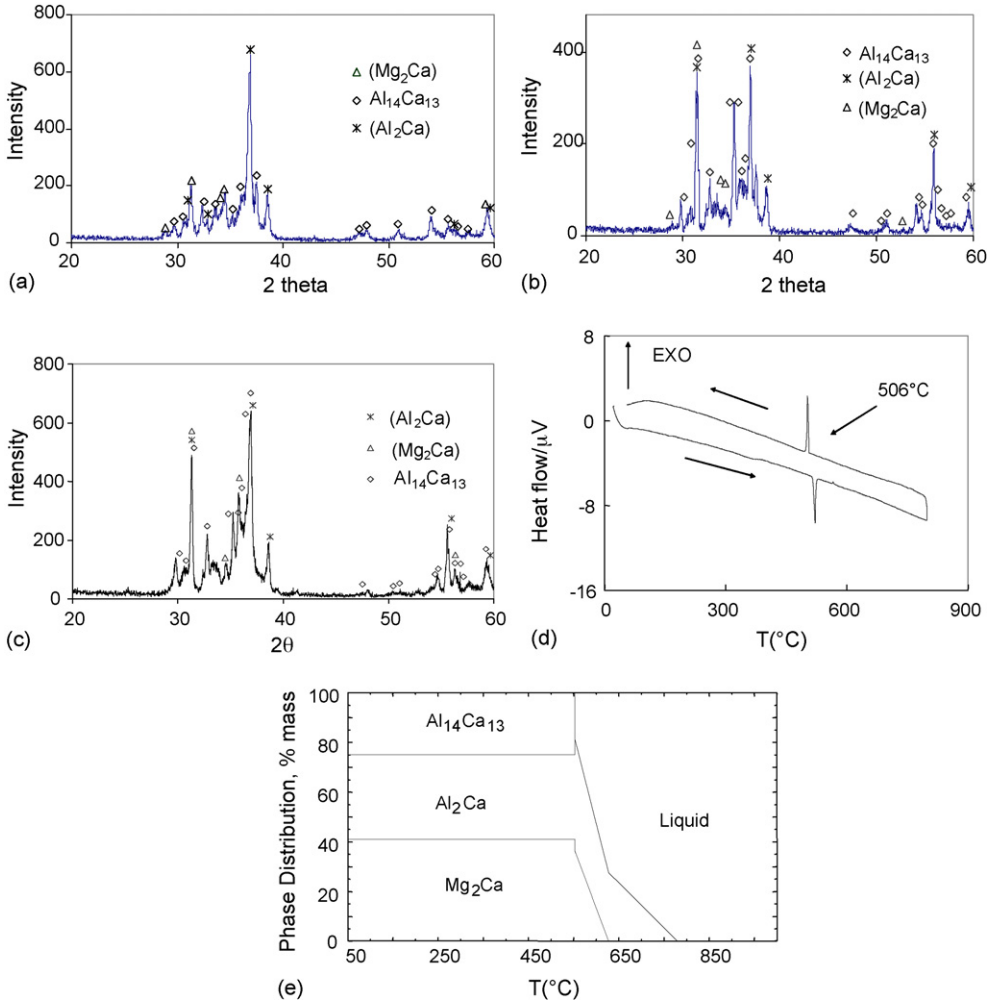

Fig. 9. (a) XRD pattern of sample 18 (44.30/23.76/31.94 wt.% Ca/Mg/Al); (b) XRD pattern of sample 19 (46.73/13.00/40.27 wt.% Ca/Mg/Al); (c) XRD pattern of sample 20 (12.65/77.46/9.89 wt.% Ca/Mg/Al); (d) DSC spectra of sample 20 and (e) phase assemblage diagram of sample 20.

that the experimental results do not agree with the thermodynamic predictions which indicates that the Mg–Al–Ca system should be reoptimized in light of the current experimental findings.

3.4. Samples in the $Al_{14}Ca_{13} + Al_2Ca + Mg_2Ca$ phase field

Samples 18–20 are selected in this phase field as shown in Fig. 1. The DSC spectra of these samples exhibited a single

Table 6
Phase contents identified by XRD at 25 °C and DSC measurements with thermodynamic analysis of the investigated samples in the $Mg_2Ca + Al_2Ca + Al_{14}Ca_{13}$ phase field (h denotes heating and c denotes cooling)

Sample	Identified phases using XRD	DSC thermal signals (°C)	Thermodynamic calculation based on the database reported in Ref. [15]	
			T (°C)	Reactions or phase boundary
18	(Al_2Ca), (Mg_2Ca) and ($Al_{14}Ca_{13}$)	506c/512h	550	$L + Al_2Ca + Mg_2Ca/Al_2Ca + Mg_2Ca + Al_{14}Ca_{13}$
		–	631	$L + Al_2Ca/L + Al_2Ca + Mg_2Ca$
		–	810	$L/L + Al_2Ca$
19	(Al_2Ca), (Mg_2Ca) and ($Al_{14}Ca_{13}$)	506c/520h	550	$L + Al_2Ca + Mg_2Ca/Al_2Ca + Mg_2Ca + Al_{14}Ca_{13}$
		–	620	$L + Al_2Ca + Mg_2Ca/L + Al_2Ca$
		–	909	$L + Al_2Ca/L$
20	(Al_2Ca), (Mg_2Ca) and ($Al_{14}Ca_{13}$)	506c/514h	550	$L + Al_2Ca + Mg_2Ca/Al_2Ca + Mg_2Ca + Al_{14}Ca_{13}$
		–	627	$L + Al_2Ca + Mg_2Ca/L + Al_2Ca$
		–	785	$L + Al_2Ca/L$

Table 7
Phase contents identified by XRD at 25 °C and DSC measurements with thermodynamic analysis in the $Mg_2Ca + Al_{14}Ca_{13} + Al_3Ca_8$ phase field

Sample	Identified phases using XRD	DSC thermal signals (°C)	Thermodynamic calculation based on the database reported in Ref. [15]	
			T (°C)	Reactions or phase boundary
21	(Al_3Ca_8), (Mg_2Ca) and $Al_{14}Ca_{13}$	–	633	$L/L + Al_2Ca$
		–	577	$L + Al_2Ca/L + Al_2Ca + Mg_2Ca$
		512h/507c	550	$L + Al_2Ca + Mg_2Ca/L + Mg_2Ca + Al_{14}Ca_{13}$
		–	491	$L + Mg_2Ca + Al_{14}Ca_{13}/A_{l3}Ca_8 + Mg_2Ca + Al_{14}Ca_{13}$

peak at 506 °C. This temperature corresponds to the extension of a Mg–Ca binary invariant transformation into the ternary system. The samples in this field could not be melted due to the high temperature required which might have caused oxidation of the samples. The XRD patterns of samples 18–20 in Fig. 9(a–c), respectively, show the peaks for (Al_2Ca), (Mg_2Ca) and $Al_{14}Ca_{13}$. The peaks for $Al_{14}Ca_{13}$ in sample 18 are weak because this sample is almost located on the Mg_2Ca–Al_2Ca borderline as can be seen in Fig. 1. Sample 19 is a bit farther away from the Mg_2Ca corner and closer to the $Al_{14}Ca_{13}$ corner than sample 20. Therefore, sample 19 showed stronger peaks for $Al_{14}Ca_{13}$ and Al_2Ca, but with weaker peaks for Mg_2Ca than sample 20. The XRD results of samples 18–20 are in agreement with their phase assemblage diagrams shown in Fig. 9(e).

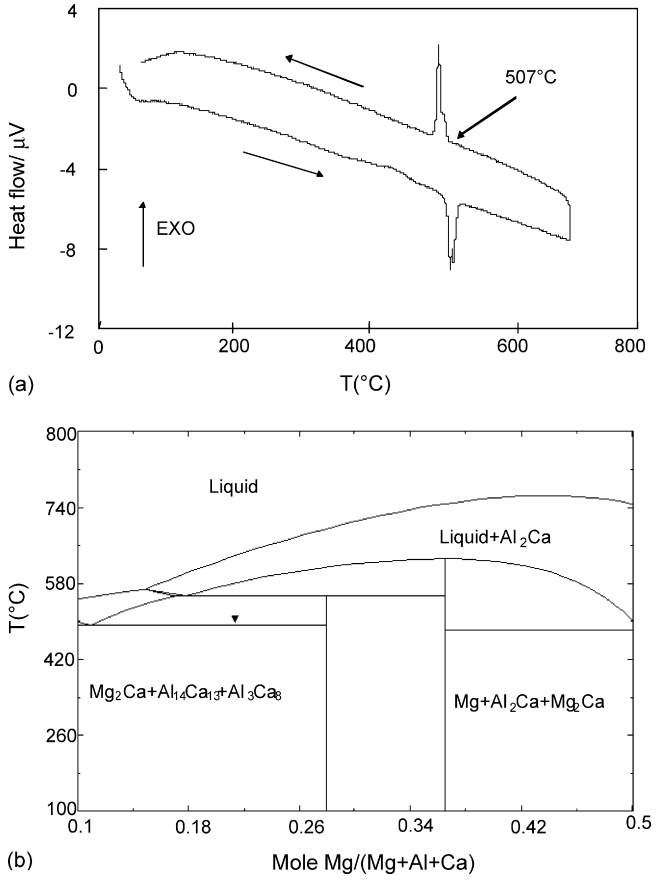

Fig. 10. (a) DSC spectra and (b) calculated vertical section at constant 30.2 at.% Al with DSC signals from cooling curve of sample 21 (59.39/15.78/24.83 wt.% Ca/Mg/Al).

The DSC measurement and their phase field detected by XRD spectra are listed in Table 6.

3.5. *Sample in the $Al_{14}Ca_{13} + Al_3Ca_8 + Mg_2Ca$ phase field*

Sample 21 was prepared in the $Al_{14}Ca_{13} + Al_3Ca_8 + Mg_2Ca$ phase field. The DSC spectra of this sample in Fig. 10(a) show a peak at 507 °C. This corresponds to the invariant transformation $L + Mg_2Ca + Al_{14}Ca_{13}/Al_3Ca_8 + Mg_2Ca + Al_{14}Ca_{13}$. The melting point of this sample could not be reached due to the high temperature required. The XRD patterns identified $Al_{14}Ca_{13}$, Al_3Ca_8 and Mg_2Ca. The XRD results of sample 21 are in agreement with the thermodynamic calculations. XRD and DSC results are summarized in Table 7 and labeled with solid triangle on the vertical section shown in Fig. 10(b).

4. Conclusion

A comprehensive investigation of the Mg–Al–Ca system has been done using XRD, DSC and metallography coupled with thermodynamic calculations. The phase transformation temperatures detected by the DSC were compared with the pertinent vertical sections. Although many samples matched well with the thermodynamic findings, a few samples showed discrepancies with the liquidus temperatures compared with the calculated values. This suggests that the Mg–Al–Ca system should be reoptimized using the experimental results obtained in this work. A ternary eutectic point in the Mg-rich corner was verified in this work and was found to occur at 513 °C. Mg_2Ca, Al_2Ca and Al_3Ca_8 were found to exist as solid solutions.

Acknowledgements

This research was carried out with the support of NSERC and NATEQ grants, Canada. The authors wish to express their appreciation for this support.

References

[1] P. Humble, Mater. Forum 21 (1997) 45–56.
[2] P. Greenfield, Magnesium, Mills and Boo Limited, London, 1972, pp. 7–19.
[3] B.L. Mordike, T. Ebert, Mater. Sci. Eng. A 302 (1) (2001) 37–45.
[4] A.A. Luo, JOM 54 (2) (2002) 42–48.
[5] J. Gröbner, D. Kevorkov, I. Chumak, R. Schmid-Fetzer, Zeitschrift fuer Metallkunde 94 (9) (2003) 976–982.
[6] B.L. Mordike, Mater. Sci. Eng. A 324 (1) (2002) 103–112.

[7] R. Ninomiya, T. Ojiro, K. Kubota, Acta Metall. Mater. 43 (2) (1995) 669–674.
[8] K. Maruyama, M. Suzuki, H. Sato, Metall. Trans. 33 (3) (2002) 875–882.
[9] O. Beffort, Ch. Hausmann, The influence of Ca-additions on the mechanical properties of T300-C-fibre/Mg (Al) Metal Matrix Composites, in: K.U. Kainer (Ed.), Magnesium Alloys and their Applications, Wiley-VCH Verlag GmbH, Weinheim, Germany, 2000, pp. 215–220.
[10] M.O. Pekguleryuz, E. Baril, Mater. Trans. 42 (7) (2001) 1258–1267.
[11] A.A. Luo, M.P. Balogh, B.R. Powell, Metall. Mater. Trans. A 33 (3) (2002) 567–574.
[12] W. Blum, P. Zhang, B. Watzinger, B.V. Grossmann, H. Lipowski, H.G. Haldenwanger, Mater. Sci. Forum 350–351 (2000) 141–150.
[13] W. Blum, P. Zhang, B. Watzinger, B.V. Grossmann, H.G. Haldenwanger, Mater. Sci. Eng. A 319–321 (2001) 735–740.
[14] A. Suzuki, N.D. Saddock, J.W. Jones, T.M. Pollock, Acta Mater. 53 (9) (2005) 2823–2834.
[15] F. Islam, M. Medraj, Can. Metall. Q. 44 (4) (2005) 523–535.
[16] K. Ozturk, Y. Zhong, Z.K. Liu, Magnesium Technology, in: Proceedings of the Symposium Held During the TMS Annual Meeting, New Orlens, LA, United States, 2001, pp. 113–117.
[17] k. Ozturk, Investigation in Mg—Al—Ca—Sr System by Computational Thermodynamics Approach Coupled with First-Principles Energetics and Experiments, PhD thesis, the Pennsylvania State University, Pennsylvania, USA, 2003.
[18] FactSage 5.3, Thermfact (Center for Research in computational Thermochemistry), Montreal, Quebec, Canada, 2003.
[19] W. Kraus, G. Nolze, PowderCell for Windows, Federal Institute for Mater. Research and Testing Berlin, 1999, Version 2.3.